RAA 2021 Vol. **21** No. **9**, 236(7pp) doi: 10.1088/1674-4527/21/9/236

http://www.raa-journal.org *http://iopscience.iop.org/raa*

***R**esearch in*
***A**stronomy and*
***A**strophysics*

Magnetar giant flare originating from GRB 200415A: transient GeV emission, time-resolved E_p – $L_{\rm iso}$ correlation and implications

Vikas Chand[1,2], Jagdish C. Joshi[1,2], Rahul Gupta[3,4], Yu-Han Yang[1,2], Dimple[3,4], Vidushi Sharma[5], Jun Yang[1,2], Manoneeta Chakraborty[6], Jin-Hang Zou[7], Lang Shao[7], Yi-Si Yang[1,2], Bin-Bin Zhang[1,2,8], Shashi Bhushan Pandey[3], Ankush Banerjee[10] and Eman Moneer[9]

[1] School of Astronomy and Space Science, Nanjing University, Nanjing 210093, China; *vikasK2@nju.edu.cn; jjoshi@nju.edu.cn; bbzhang@nju.edu.cn*
[2] Key Laboratory of Modern Astronomy and Astrophysics (Nanjing University), Ministry of Education, Nanjing 210093, China
[3] Aryabhatta Research Institute of Observational Sciences (ARIES), Manora Peak, Nainital-263002, India
[4] Department of Physics, Deen Dayal Upadhyaya Gorakhpur University, Gorakhpur 273009, India
[5] Inter University Centre for Astronomy and Astrophysics, Pune, India
[6] DAASE, Indian Institute of Technology Indore, Khandwa Road, Simrol, Indore 453552, India *manoneeta@iiti.ac.in*
[7] College of Physics, Hebei Normal University, Shijiazhuang 050024, China
[8] Department of Physics and Astronomy, University of Nevada, Las Vegas, NV 89154, USA
[9] Princess Nourah Bint Abdurhamn University, Department of Physics, KSA Riyadh 84428 Airport Road, KSA, 11671
[10] Private Astronomer

Received 2020 December 2; accepted 2021 May 3

Abstract Giant flares (GFs) are unusual bursts from soft gamma-ray repeaters (SGRs) that release an enormous amount of energy in a fraction of a second. The afterglow emission of these SGR-GFs or GF candidates is a highly beneficial means of discerning their composition, relativistic speed and emission mechanisms. GRB 200415A is a recent GF candidate observed in a direction coincident with the nearby Sculptor galaxy at 3.5 Mpc. In this work, we searched for transient gamma-ray emission in past observations by *Fermi*-LAT in the direction of GRB 200415A. These observations confirm that GRB 200415A is observed as a transient GeV source only once. A pure pair-plasma fireball cannot provide the required energy for the interpretation of GeV afterglow emission and a baryonic poor outflow is additionally needed to explain the afterglow emission. A baryonic rich outflow is also viable, as it can explain the variability and observed quasi-thermal spectrum of the prompt emission if dissipation is happening below the photosphere via internal shocks. Using the peak energy (E_p) of the time-resolved prompt emission spectra and their fluxes (F_p), we found a correlation between E_p and F_p or isotropic luminosity $L_{\rm iso}$ for GRB 200415A. This supports the intrinsic nature of E_p-$L_{\rm iso}$ correlation found in SGRs-GFs, hence favoring a baryonic poor outflow. Our results also indicate a different mechanism at work during the initial spike, and that the evolution of the prompt emission spectral properties in this outflow would be intrinsically due to the injection process.

Key words: gamma-rays: general, stars: magnetars, stars: flares, methods: data analysis

1 INTRODUCTION

Soft gamma-ray repeaters (SGRs) are young, slow-spinning magnetars, exhibiting tens to hundreds of short (duration of ms to s) repetitive bursts in a soft gamma-ray band (Duncan & Thompson 1992a; Thompson & Duncan 1995). Their spin periods range from 2 to 12 s and the corresponding spin-down ages vary between $10^3 - 10^5$ yr. During their active outburst phases, the magnetars exhibit strong flaring activities spanning a wide range of intensities and durations [1]. Magnetar flare emission activities are broadly classified into (i) short bursts ($10^{36} - 10^{41}$ erg s^{-1}) that last for a duration ranging from a few milliseconds to a few seconds, (ii) intermediate bursts ($10^{41} - 10^{43}$ erg s^{-1})

[1] https://staff.fnwi.uva.nl/a.l.watts/magnetar/mb.html

or (iii) giant flares (GFs) ($10^{44} - 10^{47}$ erg s^{-1}) lasting for several minutes (see, e.g., Kaspi & Beloborodov 2017). The GFs of SGRs are typically characterized by a short hard initial intensity spike followed by a gradual intensity decay over hundreds of seconds, during which oscillations corresponding to the spin period of the magnetar are observed. The initial strong intensity spike corresponds to a spectrally hard emission with energies greater than 60 keV (Palmer et al. 2005) lasting for typical duration of $\sim$ 0.1 s. The GF events are extremely rare and, till date, only three confirmed GFs have been discovered since 1979 from SGRs: SGR 0526–66 (Mazets et al. 1979, 1982), SGR 1900+14 (Cline et al. 1998; Hurley et al. 1999; Kouveliotou et al. 1999; Mazets et al. 1999b) and SGR 1806–20 (Mereghetti et al. 2005; Palmer et al. 2005; Hurley et al. 2005; Frederiks et al. 2007a), respectively. Another possible candidate GF was detected, SGR 1627–41 (Mazets et al. 1999a; Woods et al. 1999), but not confirmed. Because of their intense gamma-ray luminosity and spectral characteristics, distant (extragalactic) SGR-GFs have long been proposed to contribute at least a subset of the observed short Gamma-ray Bursts (sGRBs) (Hurley et al. 2005). GRB 051103 (Frederiks et al. 2007b; Ofek et al. 2006) and GRB 070201 (Mazets et al. 2008; Ofek et al. 2008) in the past have been proposed as candidates of GF-sGRBs. GRB 200415A is the first extragalactic GF candidate observed by the *Fermi* space observatory (Yang et al. 2020; Zhang et al. 2020).

The physical mechanism of GFs is still a puzzle despite many investigations (Thompson & Duncan 1995; Lyutikov 2003; Parfrey et al. 2013). The relation between the time-integrated properties of GFs (Zhang et al. 2020) and their evolution during a GF (this work) can provide insights into these. Afterglow emissions are another possible electromagnetic counterpart of GFs. Previously, radio afterglow emissions have been detected from two GF sources (Frail et al. 1999; Gaensler et al. 2005; Cameron et al. 2005). For GRB 200415A, emission recorded by the *Fermi*-Large Area Telescope (LAT) was reported (Omodei et al. 2020). In the *Fermi* era, GRB 200415A is the first GF candidate, and therefore the observed LAT emission would be the first detection of GeV radiation from magnetars. Prior to this source, GeV radiation was not detected from magnetars, and only upper limits on flux $\sim 10^{-12} - 10^{-11}$erg cm^{-2} s^{-1} were known (Li et al. 2017). Hence, it forms an exquisite opportunity to examine the energetics and origin of this emission also in conjunction with observed prompt emission properties.

2 ANALYSIS

2.1 Prompt Emission

The isotropic equivalent energy of the GF and peak luminosity, assuming its association with the Sculptor galaxy (NGC 253 at 3.5 Mpc), are estimated as $E_{\gamma,\rm iso} = 1.36^{+0.14}_{-0.13} \times 10^{46}$ erg and $L_{\gamma,\rm p,iso} = 1.62^{+0.21}_{-0.16} \times 10^{48}$ erg s^{-1}, respectively (Yang et al. 2020). Therefore, the radiation luminosity for the time-integrated duration of 0.2 s is $\sim 7 \times 10^{46}$ erg s^{-1}. In the time-dependent spectral analysis by Yang et al. (2020), for interval –5 – 120 ms, blackbody (BB), multicolor-blackbody (mBB) or a quasi-thermal spectrum is a preferred fit. We further resolved their second time-bin where the best fit was mBB based on signal to noise ratio of $\sim$ 20. The spectral parameters of the modeled powerlaw with an exponential cutoff (CPL) are presented in Table 1.

2.2 The *Fermi*-LAT Observation of GRB 200415A

We retrieved the photon event data files and the spacecraft history files (pointing and livetime history) from the LAT data server[2] at the updated localization of the LAT observations, J2000 RA, Dec = 11.07, –25.02 degrees (Omodei et al. 2020). The data are obtained in a spatial radius of 40° and energy range of 100 MeV to 300 GeV. We selected a 12° region of interest (ROI) centered at the burst location and also constrained the zenith angle to 100° to avoid contamination from the Earth's limb. We selected the cleaner "`Pass 8 source`" class (`evclass` = 128 and `evtype` = 3) with response function `P8R3_SOURCE_V2`. The corresponding model for extragalactic diffuse gamma-ray background `iso_P8R3_SOURCE_V2.txt` is used and for the Galactic contribution, diffuse gamma-ray emission is estimated utilizing the official Galactic interstellar emission model `gll_iem_07.fits`.

The analyses are carried out with the following objectives: (1) Ascertain the detection of a transient emission, for this purpose we choose the data in a relatively small interval of 10 000 s before the trigger-time, and from the trigger-time to 1000 s. (2) Study the nature of the transient emission, the data are analyzed between 5 d prior to the trigger-time (t_0) to 5 d after. (3) After this analysis, we aim to confirm if there is any other transient emission before this emission in the past observations of *Fermi*-LAT. A computationally less expensive approach is followed. The data are first analyzed in an interval with a bin size of six months, which is then used to extrapolate to set a reference limit on flux, and the analysis is finally carried out in an interval of bin size of 2 d for 11.5 yr of data.

We performed unbinned likelihood analysis and have displayed the residual TS map in Figure 1 without contribution from this source. In a short duration of 500 s and 1000 s, the analyses indicate that the GRB is detected with test statistic (TS) values of 27 and 26, respectively. We plotted the TS map in a 16° × 16° region at 0.2° resolution

[2] https://fermi.gsfc.nasa.gov/cgi-bin/ssc/LAT/LATDataQuery.cgi

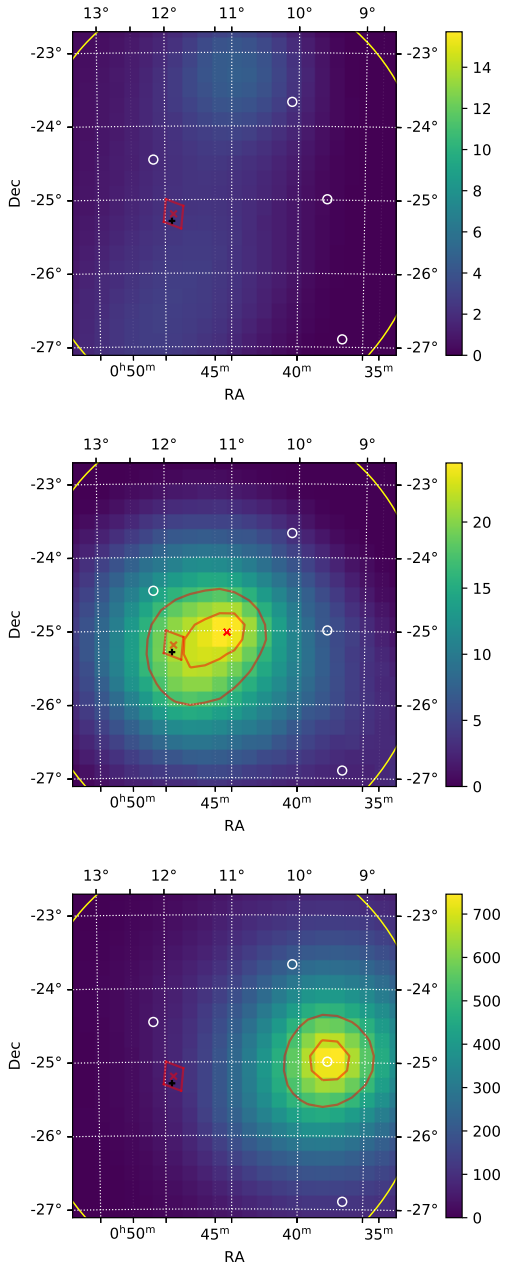

Fig. 1 The TS map in a $16° \times 16°$ region at $0.2°$ resolution (zoomed for better visualization). The color-bars on each image represent the TS values. The IPN triangulation localization-region of the GRB is bounded by red lines centered at the cross. The GRB is associated with the Sculptor Galaxy (NGC 253) marked with a plus sign. *Top*: The TS map from –10 000 to 0 s. There is no significant emission within the IPN triangulation region during this interval. *Middle*: TS map from 0 – 1000 s. A maximum TS value of 26 is obtained at the GRB location, signaling a $\sim 5\sigma$ detection. The 68% and 90% confidence levels are plotted in red contours. Other known sources from the *Fermi*-LAT Fourth Source Catalog are marked by open circles. A bigger circle with a 3° radius centered on the updated LAT localization is drawn for reference. *Bottom*: The location of the many transient detections. The signal with significance of ≈ 15 is depicted.

(zoomed for better visualization). The color-bars on each image represent the TS values. The GRB is associated with the Sculptor Galaxy (NGC 253). A maximum TS value of 26 is obtained at the GRB location from 0 – 1000 s duration, signaling a $\sim 5\sigma$ detection. Confidence levels (68% and 90%) are plotted. Other known sources from the *Fermi*-LAT Fourth Source Catalog are marked by open circles.

On a scale of 1 d, the photons are still sparsely distributed and thus unbinned likelihood analysis is performed using `gtlike`. The GRB contribution to the observed statistics is evaluated applying a `powerlaw2`[3] model, and flux (photon and energy flux) is calculated in the energy range 0.1 – 10 GeV. The upper limits are obtained by assuming a spectral shape with an index equal to –2. LAT detected high energy photons in the first temporal bin (firebrick colored datapoint in Figure 2(a)) after the trigger-time. To set a reference limit on flux from the direction of the observed LAT emission, we also analyzed the 11.5 yr of *Fermi*-data employing binned likelihood analysis in bin-sizes of six months. The spectral parameters of the models for the sources within 3° centered on the GRB position (as marked by the yellow circle in Figure 1) are kept free for the likelihood analysis. The flux upper limits and corresponding luminosity are plotted in Figure 2 (b).

We binned the data since 2009–01–01 UTC in a bin size of 2 d. Known point sources in the ROI are also included[4] and spectral parameters are fixed to the values reported in the *Fermi*-LAT Fourth Source Catalog (Abdollahi et al. 2020). The significance of the emission $\sim\sqrt{TS}$ is plotted in Figure 2(c). The flux averaged over the six month upper limits (blue dashed line in Fig. 2(b)) is extrapolated (e.g. as in Yang et al. 2019a) to a bin size of 2 d and displayed as a in red line in Fig. 2(d)). We also feature the TS map at the location of the many detections in the bottom panel of Figure 1. Other detections with TS $>$ 16 represented in Figure 2 in firebrick color are also at this location and therefore only one with the largest significance (significance $\approx$ 15) is shown for a reference. Here, the IPN localization area is not encircled by the confidence contours as in the case of the emission observed $\sim$ 19 s after the *Fermi* trigger.

3 RESULTS

An injected GF gamma-ray luminosity of $L_\gamma \sim 7 \times 10^{46}$ erg s^{-1} near the neutron star (radius $R_0 \sim 10^6$ cm) produces a fireball, which expands due to its own radiation pressure. The optical depth for $\gamma-\gamma$ interaction is $\tau_{\gamma\gamma} \gtrsim E\sigma_T/(4\pi e_\gamma R_0 ct) \approx 1.36 \times 10^{11} E_{46.13} R_{0,6}^{-1} t_{-0.7}^{-1}$.

[3] https://fermi.gsfc.nasa.gov/ssc/data/analysis/scitools/source_models.html#PowerLaw2

[4] user contributed software https://fermi.gsfc.nasa.gov/ssc/data/analysis/user/python3/make4FGLxml.py

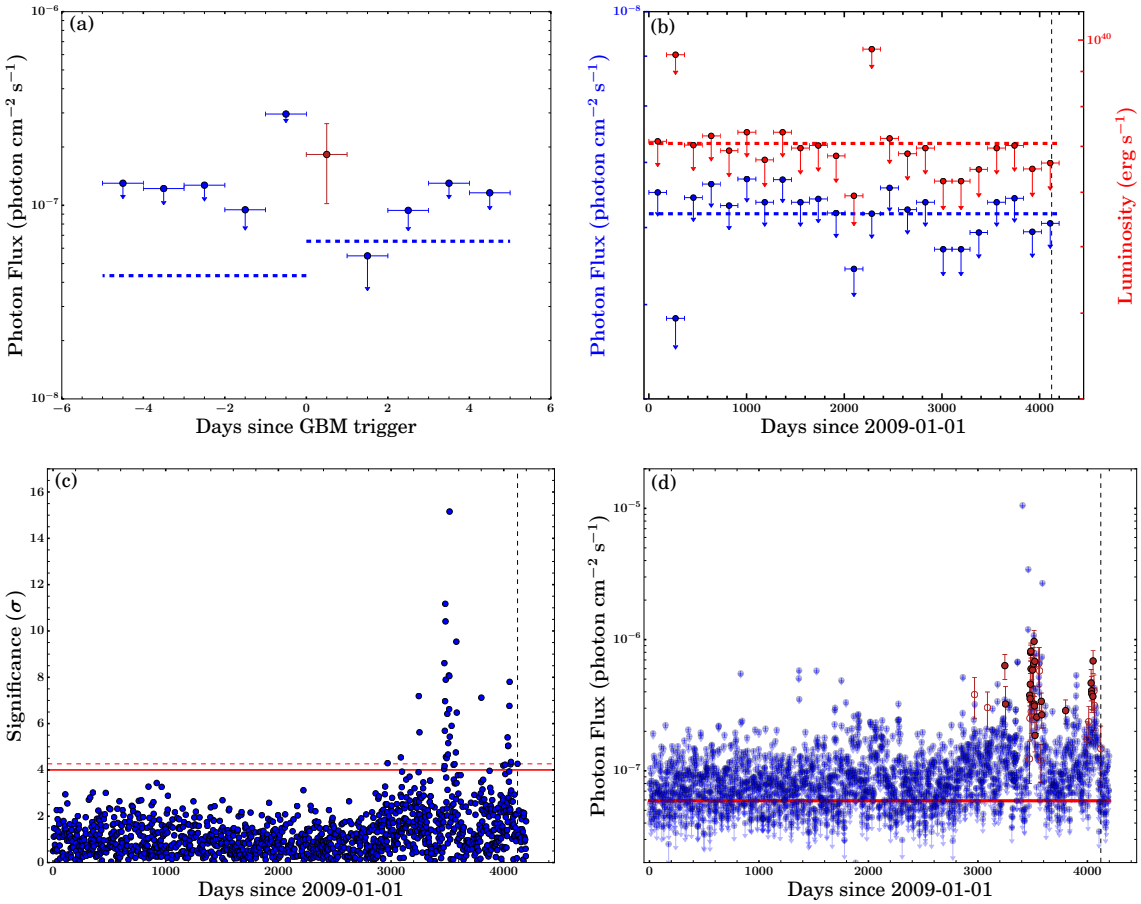

Fig. 2 (a) Photon fluxes for GRB 200415A from t_0-5 d to t+5 d with bin size 1-d. The horizontal blue dashed lines correspond to the total flux limit for combined bins from 1 to 5 d before and after the trigger-time. (b) The photon fluxes (*blue*) and corresponding luminosities (*red*) upper limits from LAT observations of GRB 200415A location with a half-year bin. The blue and red horizontal dashed lines show the averaged values of the 11.5 yr upper limits of photon fluxes and luminosities, respectively. (c) Distribution of significance with 2 d temporal binning. The solid red line signifies the TS equal to 16 and the dashed line indicates TS of the source during bin after trigger-time. (d) *Fermi*-LAT flux light curve for 11.5 yr of observations in the direction of GRB 200415A. Blue circles mark the upper limits (TS $<$ 16) and firebrick circles show the detection of high energy photons (TS $>$ 16). Open and filled firebrick circles signify the TS values 16 $<$ TS $<$ 25 and TS $>$ 25, respectively. The red solid line represents the 2 d photon flux upper limit extrapolated from the average value of the 11.5 yr upper limits (Yang et al. 2019b). The vertical black dashed lines in (b), (c) and (d) indicate *Fermi* GBM trigger-time.

Here, we used notation $X = 10^n X_n$, and σ_T is the Thompson cross-section, $t \sim 0.2 t_{-0.7}$ s is the duration of the prompt emission, and $e_\gamma \sim 900$ keV is the mean energy obtained from time-integrated spectral fit. This huge optical depth creates a radiation and $e^{\pm}$ pair dominated plasma, with initial temperature $T_0 \approx (E/4\pi R^2 \sigma t)^{1/4} \approx 270 E_{46.13}^{1/4} R_{0,6}^{-1/2} t_{-0.7}^{-1/4}$ keV (Paczynski 1986; Nakar et al. 2005). The Lorentz factor of this plasma increases with radius $\Gamma \propto R$ and comoving temperature decreases as inversely proportional to radius $T \propto R^{-1}$ (Goodman 1986; Paczynski 1986; Shemi & Piran 1990; Duncan & Thompson 1992b; Piran et al. 1993; Meszaros et al. 1993; Katz 1996). During this evolution, at some stage, pair production is negligible and we can estimate number of pairs $N_\pm \approx 4 \times 10^{44} E_{46.13}^{3/4} R_{0,6}^{-1/2} t_{-0.7}^{1/4}$ (Nakar et al. 2005). Even after this stage, photons are coupled to the pairs through scattering, which accelerate the pair plasma to a bulk Lorentz factor $\Gamma_\pm$. The bulk Lorentz factor and kinetic energy of the pair plasma are given by $\Gamma_\pm = (E\sigma_T/4\pi c^3 t m_e R_0)^{1/4} \approx 620 E_{46.13}^{1/4} R_{0,6}^{-1/4} t_{-0.7}^{-1/4}$ and $E_\pm = N_\pm \Gamma_\pm m_e c^2 \approx 1.9 \times 10^{41}$erg, respectively (Nakar et al. 2005).

For the afterglow observed by *Fermi*-LAT in the energy range 0.1-10 GeV, for 0-1000 s, we calculate energy flux, which is $\sim (3.78 \pm 2.24) \times 10^{-09}$ erg cm^{-2} s^{-1}. This component has total energy $E_{LAT} \approx 5.53 \times 10^{45}$ erg, however, the kinetic energy left in pair plasma is $\sim 10^{-5}$ of the energy of GeV emission. This also infers that the

observed LAT afterglow cannot be powered by ejecta with pure pair fireball composition.

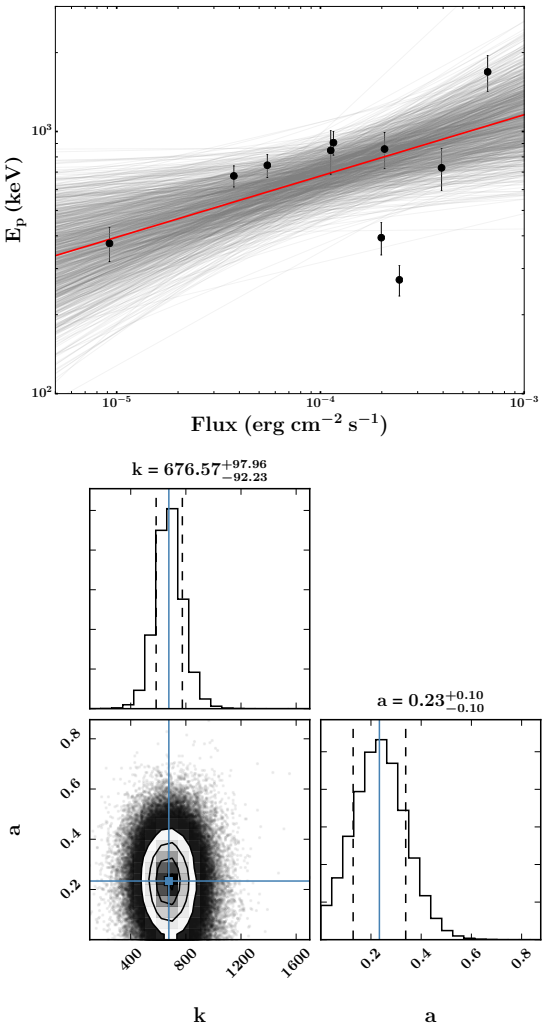

Fig. 3 *Top panel:* Time-dependent $E_p - F_p$ correlation for GRB 200415A. The red line represents the best fit. *Bottom panel:* Corner plot features the results obtained from a Markov Chain Monte Carlo (MCMC) simulation for a simple powerlaw model. a and k represent the index and norm of the powerlaw relation, respectively.

In addition to radiation and $e^{\pm}$ pairs, the fireball can also be loaded with baryons, having baryon injection rate $\dot{M}$ and total burst luminosity $L_0 = L_\gamma/\xi_\gamma$, where ξ_γ is the conversion efficiency of total burst luminosity into gamma rays, and the outflow evolution is parameterized in terms of the dimensionless entropy $\eta = L_0/\dot{M}c^2$ (Shemi & Piran 1990; Ioka et al. 2005b). We will consider two possible loading cases, (i) baryonic poor (BP) outflow, when $\eta > \eta_*$, where $\eta_* = (L_0\sigma_T/4\pi m_p c^3 R_0)^{1/4} = 91 L_{0,46.8}^{1/4} R_{0,6}^{-1/4}$ is the critical entropy (Mészáros & Rees 2000). In the BP case, the photosphere is in an accelerating phase and photospheric radius is below the saturation radius (Mészáros & Rees 2000). The observed temperature is $T_{ph} = T_0 \sim 270$ keV and quasi-thermal emission has peak at ∼900 keV. The emission is radiated away from the photospheric radius and the final Lorentz factor would be $\Gamma_f = \eta_* \approx 90$. From the observed afterglow and the energy remaining in the baryons, we have $\eta = \xi_L(E/E_{LAT}) \times \eta_*$, where ξ_L is the efficiency of conversion of the kinetic energy (E_K) into the GeV afterglow.

Since $\xi_L < 1$, we find $\eta < 227$. Using this η, we can constrain the baryonic load, and obtain a value of $M > E/\eta c^2 \approx 6.65 \times 10^{22}$ gm. Utilizing $\eta > \eta_*$, we also have an upper limit on baryonic load $M < 1.66 \times 10^{23}$ gm. In the BP case, therefore, considering the observed afterglow we constrain the baryonic load to be 6.65×10^{22} gm $< M < 1.66 \times 10^{23}$ gm.

The afterglow discussed here is produced in a forward shock when the ejecta inevitably penetrates through the circumburst medium. At the deceleration time of the external forward shock, the Lorentz factor is one half of the initial Lorentz factor, assuming that the peak time is the observed time when the first photon (probability ≥ 0.9) from the source is received. Using the initial Lorentz factor we can constrain the density of the ambient medium (Sari & Piran 1999). For $\Gamma_0 \sim 45 E_{K,47}^{1/8} n_0^{-1/8} t_{\gamma,2}^{-3/8}$ and $\eta_* = 91$, $t_\gamma \sim t_{start} = t_{i,obs} \sim 19$ s (time when first photon with probability ≥ 0.9 is received) and implementing $E_K = (\eta_*/\eta)E_{\gamma,iso}$, $\Gamma_0 = \eta_*$, we found $n < 4 \times 10^{-4}$ cm^{-3}. Here we have assumed peak time to be the start of the LAT emission. The density would be lower, if peak occurs later than this.

The other case is (ii) baryonic rich (BR) ejecta, here the photosphere is in a coasting phase (Nakar et al. 2005). The emission observed in *Fermi*-GBM has a minimum variability timescale (∼ 2 ms, Yang et al. 2020), which is one of the extreme values when compared to a sample of GRBs (Yang et al. 2020). Thermal emission from internal shocks can arise if it occurs below the photosphere (Rees & Mészáros 2005). In such a case, the kinetic energy left in the ejecta can be ∼10 times the radiation energy and a jet configuration or atypical parameters are required to explain the afterglows (e.g., as in the case of SGR 1806–20, Ioka et al. (2005a)). The temperature/peak energy tracks the photon flux (Yang et al. 2020). Such an evolution can be a result of many multiple superimposed pulse evaluations (e.g., as discussed in reference to GRBs by Preece et al. 2016).

We note that very recently Zhang et al. (2020) discussed the magnetar GF origin of the emission in GRB 200415A. For the magnetar GF candidates, they found a correlation similar to the Amati correlation in GRBs. Further, they discussed the outflow composition and energetics following the standard analysis (e.g., in

Table 1 Time-dependent Spectral Analysis Results Based on GBM Observations, Using CPL Model

Sr. no.	Intervals (s)	$\Gamma_{\rm ph}$	$E_{\rm p}$, (keV)	Flux (10^{-4} erg cm^{-2} s^{-1})
1	(–0.005, –0.003)	$0.36^{+0.29}_{-0.31}$	$393.53^{+72.77}_{-38.06}$	$1.99^{+0.50}_{-0.39}$
2[a]	(–0.003, -0.0024)	$1.54^{+1.02}_{-0.52}$	$271.68^{+44.14}_{-27.83}$	$2.44^{+0.79}_{-0.58}$
3[a]	(–0.0024, -0.001)	$0.16^{+0.32}_{-0.23}$	$726.84^{+146.29}_{-118.88}$	$3.93^{+1.26}_{-1.06}$
4	(–0.001, 0.001)	$-0.00^{+0.26}_{-0.16}$	$1688.27^{+304.76}_{-224.37}$	$6.61^{+2.19}_{-1.66}$
5	(0.001, 0.005)	$0.60^{+0.46}_{-0.26}$	$857.35^{+134.64}_{-132.59}$	$2.06^{+0.65}_{-0.56}$
6	(0.005, 0.010)	$1.67^{+0.88}_{-0.68}$	$847.03^{+198.13}_{-121.32}$	$1.12^{+0.48}_{-0.36}$
7	(0.010, 0.020)	$0.53^{+0.30}_{-0.20}$	$907.19^{+99.54}_{-89.61}$	$1.16^{+0.26}_{-0.20}$
8	(0.020, 0.040)	$0.63^{+0.38}_{-0.20}$	$743.53^{+74.67}_{-75.94}$	$0.55^{+0.11}_{-0.10}$
9	(0.040, 0.080)	$0.31^{+0.23}_{-0.16}$	$676.90^{+66.68}_{-58.29}$	$0.38^{+0.07}_{-0.05}$
10	(0.080, 0.120)	$0.65^{+0.52}_{-0.35}$	$374.23^{+63.24}_{-46.83}$	$0.09^{+0.03}_{-0.02}$

a: newer bins.

reference to GFs Nakar et al. 2005; Ioka et al. 2005a; Dai et al. 2005; Wang et al. 2005). They ruled out BR outflow based on the relation between the observed temperature and isotropic energy.

Such a correlation, if intrinsic, should also be present between the considered observables in the time-dependent data (in case of GRBs, e.g., Frontera et al. 2012). We find that hints of such a correlation between the peak energy E_p and isotropic luminosity $L_{\rm iso}$ are present with Pearson linear correlation coefficient r = 0.67 and p-value = 0.03;

$$\left(\frac{E_p}{1\,\rm keV}\right) \approx 619^{+93}_{-87}\left(\frac{L_{\rm iso}}{10^{47}\rm erg\ s^{-1}}\right)^{0.23\pm0.10}. \quad (1)$$

In another form, we have $\log(E_{p,0}) \sim 2.8 + (0.23 \pm 0.10)\log(L_{\rm iso,47})$ which is consistent with their results ($E_p \sim E_{\rm iso}^{1/4}$). The scaling relation between E_p and peak flux F_p is

$$\left(\frac{E_p}{1\,\rm keV}\right) \approx 676^{+98}_{-92}\left(\frac{F_p}{10^{-4}\,\rm erg\ cm^{-2}\ s^{-1}}\right)^{0.23\pm0.10}. \quad (2)$$

For a BP outflow, the temperature observed is the photospheric temperature ($T \sim T_0$). This implies the observed evolution in the case of this source is intrinsic to the injection process rather than the dynamics of the outflow. Alternatively, multiple thermal shells with varying temperatures might be injected from the central source. This is also evident from the observed BB spectrum in bins of size $\sim$ 4 ms or quasi-thermal spectrum in larger bins. The dispersion in the correlation can arise in such a case from other parameters, which may vary within injections, such as radius R_0 at which injection occurs. The first three points in the time-dependent spectra during –0.005 to –0.001 s are farther from the fitted correlation (assuming an uptrend is more evident). If we exclude these three datapoints, both the correlation and significance are strengthened. The Pearson linear correlation coefficient is r = 0.96 (p = 0.0008), and linear correlation between the logarithmic values of the E_p and $L_{\rm iso}$ is 0.97 (0.0003). The new relation is ($E_{p,0} \approx 752^{+35}_{-35}L_{\rm iso,47}^{0.31\pm0.04}$).

4 DISCUSSION

We have systematically studied the afterglow emission in the case of the GF candidate GRB 200415A. No other transient emission in the direction of the GRB was detected in the past 11.5 yr of *Fermi* observations than the one detected $\sim$ 19 s after the GBM trigger. We also systematically arrive at the conclusions that the high energy emission as observed in *Fermi*-LAT is produced in a BP fireball when the ejecta runs into the ambient medium. In this scenario, we have constrained the baryonic load in the ejecta. We assumed that the ejecta expands into a constant density medium and, using the initial Lorentz factor of the ejecta, onset time of the GeV afterglow and energy of the ejecta, we have constrained the density of the ambient medium.

The time-averaged peak energy (E_p) and isotropic equivalent energy $E_{\rm iso}$, in a sample of SGR-GF candidates, are correlated (Zhang et al. 2020). We found a time-dependent correlation between E_p and isotropic luminosity ($L_{\rm iso}$) for GRB 200415A (Eq. 1). The existence of the time-dependent relation between the E_p and $L_{\rm iso}$ emitted by the source similar to the time-averaged correlation found for the GF candidates favors a BP outflow over a BR outflow (Zhang et al. 2020). Moreover, this also implies that the observed evolution in the peak energy is intrinsic to the injection process. Finally, our results show that the correlation is tighter if we exclude the initial 4 ms (first three time intervals in Table 1), implying a different emission mechanism is at work during this period.

The physical mechanisms responsible for the GFs have eluded a complete understanding despite many investigations (Thompson & Duncan 1995, 2001; Lyutikov 2003; Parfrey et al. 2013; Takamoto et al. 2014). The spectral evolution and the variability during a GF indicate the complex nature of the central source. This can be probed by a search for other observed features, e.g. QPOs that originate in a magnetic reconnection scenario and seismic modes in the magnetar crust which developed during the GF and which are aided by the intense magnetic

field (Strohmayer & Watts 2006). Finally, we note that for nearby GF-candidate GRBs with unknown distance, the power of the scaling (Eq. (2)) relation discussed in this article is that one can utilize the relation between the peak energy and flux for distinguishing it from sGRBs.

DATA AVAILABILITY

The data underlying this article will be shared on reasonable request to the corresponding author.

Acknowledgements We thank A.R. Rao, K. Ioka and X.Y. Wang for discussions. B.B.Z. acknowledges support by the Fundamental Research Funds for the Central Universities (14380035). This work is supported by National Key Research and Development Programs of China (2018YFA0404204), the National Natural Science Foundation of China (Grant Nos. 11833003, U1838105 and U1831135) and the Program for Innovative Talents, Entrepreneur in Jiangsu, and the Strategic Priority Research Program on Space Science, the Chinese Academy of Sciences (Grant No. XDB23040400). RG and SBP acknowledge BRICS grant DST/IMRCD/BRICS/PilotCall1/ProFCheap/2017(G) for the financial support.

Softwares used: Astropy (Astropy Collaboration et al. 2013), Emcee (Foreman-Mackey et al. 2013)

References

Abdollahi, S., Acero, F., Ackermann, M., et al. 2020, ApJS, 247, 33
Astropy Collaboration, Robitaille, T. P., Tollerud, E. J., et al. 2013, A&A, 558, A33
Cameron, P. B., Chandra, P., Ray, A., et al. 2005, Nature, 434, 1112
Cline, T. L., Mazets, E. P., & Golenetskii, S. V. 1998, IAU Circ., 7002, 1
Dai, Z. G., Wu, X. F., Wang, X. Y., et al. 2005, ApJL, 629, L81
Duncan, R. C., & Thompson, C. 1992a, ApJL, 392, L9
Duncan, R. C., & Thompson, C. 1992b, ApJL, 392, L9
Foreman-Mackey, D., Hogg, D. W., Lang, D., & Goodman, J. 2013, PASP, 125, 306
Frail, D. A., Kulkarni, S. R., & Bloom, J. S. 1999, Nature, 398, 127
Frederiks, D. D., Golenetskii, S. V., Palshin, V. D., et al. 2007a, Astronomy Letters, 33, 1
Frederiks, D. D., Palshin, V. D., Aptekar, R. L., et al. 2007b, Astronomy Letters, 33, 19
Frontera, F., Amati, L., Guidorzi, C., et al. 2012, ApJ, 754, 138
Gaensler, B. M., Kouveliotou, C., Gelfand, J. D., et al. 2005, Nature, 434, 1104
Goodman, J. 1986, ApJL, 308, L47
Hurley, K., Cline, T., Mazets, E., et al. 1999, Nature, 397, 41
Hurley, K., Boggs, S. E., Smith, D. M., et al. 2005, Nature, 434, 1098
Ioka, K., Kobayashi, S., & Zhang, B. 2005a, ApJ, 631, 429
Ioka, K., Razzaque, S., Kobayashi, S., & Mészáros, P. 2005b, ApJ, 633, 1013
Kaspi, V. M., & Beloborodov, A. M. 2017, ARA&A, 55, 261
Katz, J. I. 1996, ApJ, 463, 305
Kouveliotou, C., Strohmayer, T., Hurley, K., et al. 1999, ApJL, 510, L115
Li, J., Rea, N., Torres, D. F., & de Oña-Wilhelmi, E. 2017, ApJ, 835, 30
Lyutikov, M. 2003, MNRAS, 346, 540
Mazets, E. P., Aptekar, R. L., Butterworth, P. S., et al. 1999a, ApJL, 519, L151
Mazets, E. P., Cline, T. L., Aptekar', R. L., et al. 1999b, Astronomy Letters, 25, 635
Mazets, E. P., Golenetskii, S. V., Gurian, I. A., & Ilinskii, V. N. 1982, Ap&SS, 84, 173
Mazets, E. P., Golentskii, S. V., Ilinskii, V. N., et al. 1979, Nature, 282, 587
Mazets, E. P., Aptekar, R. L., Cline, T. L., et al. 2008, ApJ, 680, 545
Mereghetti, S., Götz, D., von Kienlin, A., et al. 2005, ApJL, 624, L105
Meszaros, P., Laguna, P., & Rees, M. J. 1993, ApJ, 415, 181
Mészáros, P., & Rees, M. J. 2000, ApJ, 530, 292
Nakar, E., Piran, T., & Sari, R. 2005, ApJ, 635, 516
Ofek, E. O., Kulkarni, S. R., Nakar, E., et al. 2006, ApJ, 652, 507
Ofek, E. O., Muno, M., Quimby, R., et al. 2008, ApJ, 681, 1464
Omodei, N., Piron, F., Axelsson, M., et al. 2020, GRB Coordinates Network, 27597, 1
Paczynski, B. 1986, ApJL, 308, L43
Palmer, D. M., Barthelmy, S., Gehrels, N., et al. 2005, Nature, 434, 1107
Parfrey, K., Beloborodov, A. M., & Hui, L. 2013, ApJ, 774, 92
Piran, T., Shemi, A., & Narayan, R. 1993, MNRAS, 263, 861
Preece, R., Goldstein, A., Bhat, N., et al. 2016, ApJ, 821, 12
Rees, M. J., & Mészáros, P. 2005, ApJ, 628, 847
Sari, R., & Piran, T. 1999, ApJ, 520, 641
Shemi, A., & Piran, T. 1990, ApJL, 365, L55
Strohmayer, T. E., & Watts, A. L. 2006, ApJ, 653, 593
Takamoto, M., Kisaka, S., Suzuki, T. K., & Terasawa, T. 2014, ApJ, 787, 84
Thompson, C., & Duncan, R. C. 1995, MNRAS, 275, 255
Thompson, C., & Duncan, R. C. 2001, ApJ, 561, 980
Wang, X. Y., Wu, X. F., Fan, Y. Z., et al. 2005, ApJL, 623, L29
Woods, P. M., Kouveliotou, C., van Paradijs, J., et al. 1999, ApJL, 519, L139
Yang, J., Chand, V., Zhang, B.-B., et al. 2020, ApJ, 899, 106
Yang, Y.-H., Zhang, B.-B., & Zhang, B. 2019a, ApJL, 875, L19
Yang, Y.-H., Zhang, B.-B., & Zhang, B. 2019b, ApJL, 875, L19
Zhang, H.-M., Liu, R.-Y., Zhong, S.-Q., & Wang, X.-Y. 2020, ApJL, 903, L32